https://doi.org/10.3311/PPch.13591

Periodica Polytechnica Chemical Engineering

The Effect of the Chemical Composition to the End-Properties of Ceramic Dispersed Strengthened 316L/Y_2O_3 Composites

Haroune Rachid Ben Zine[1,2], Katalin Balázsi[2], Csaba Balázsi[2*]

[1] Doctoral School on Materials Sciences and Technologies, Óbuda University, Bécsi str. 96/B, H-1034 Budapest, Hungary
[2] Centre for Energy Research, Hungarian Academy of Sciences, Konkoly-Thege M. str. 29-33, H-1121 Budapest, Hungary
[*] Corresponding author, e-mail: balazsi.csaba@energia.mta.hu

Received: 12 December 2018, Accepted: 18 March 2019, Published online: 02 April 2019

Abstract

In this paper the influence of chemical composition to the end-properties of ceramic dispersed strengthened 316L/Y_2O_3 composites ceramic has been studied. Two various compositions were studied and compared to reference 316L sintered sample. These two compositions are 316L/0.33 wt% Y_2O_3 and 316L/1 wt% Y_2O_3. The high-efficient attrition milling has been used for grain size reduction and oxide distribution in the austenitic matrices. Spark Plasma Sintering (SPS) was used as fast compaction method of the milled powders in order to avoid excessive grain growth. In this work it was found that changing the chemical composition by increase of the Y_2O_3 addition in the composite matrix improves the milling efficiency, increases the hardness of the 316L and reduces significantly the wear rate.

Keywords

chemical composition, 316L/Y_2O_3 composite, Spark Plasma Sintering

1 Introduction

Spark Plasma Sintering (SPS) has been successfully used for the densification of a wide variety of materials (ceramic [1, 2], metals and alloys [3, 4], polymer and composites [5, 6]). Balázsi et al. [7] used as first SPS to realize nanostructured steel compacts. Many researchers studied the effect of yttria addition on the structural and mechanical properties of the steel where it was found that ultrafine yttria particles can improve significantly the hardness of steel, also its strength at high temperatures [8]. Composites with small particles exhibit higher strength because of their higher joining zone which is an effective heat source [9]. The interaction between the yttria and the steel matrix increases the diffusion of this last which increases the densification of steel, however, 12wt% or higher content of yttria will not improve the densification due to the agglomeration of yttria [10]. Oxides with Y and Cr are influencing the porosity having a direct effect on the oxidation rate in steel composites [11]. A composite with high content of yttria nano particles results in a delay in the 316L sintering, the yttria nano particles agglomerate together when sintered at lower temperatures [12]. The oxides can enhance the upper temperature limit in mechanical creep strength with 100 C° at least [13]. Lindau et al. [14] studied the effect of 0.3 % and 0.5 % yttria on the mechanical properties of the EUROFER 97 at high temperatures where it was found that the yttria improved all of the yield strength, ductility and the creep strength. Baek et al. [15] studied the hydrogen susceptibility of nano-sized Y_2O_3 dispersed strengthened 316L austenitic steel, they found that hydrogen didn't affect the yield strength and the elastic modulus of the 316L. Hutař et al. [16] studied the small fatigue crack propagation in Y_2O_3 strengthened steels and they found that yttria content has no significant effect to the crack propagation. Kumar et al. [17] studied the effect of Y_2O_3 and ZrO_2 on the microstructure and mechanical properties of nano-ODS (oxide dispersion strengthened steel) where it was found that the hot pressed Y_2O_3 containing ODS steels show higher ultimate tensile strength (UTS) comparing to the ZrO_2 containing ODS and it shows even higher UTS values when compared with ZrO_2. The yttria content under 0.6wt% improves the oxidation resistance by forming a stable oxide scale and improving the adhesion, while higher amounts of yttria results in segregation of this last, The yttria addition tends to decrease the bending strength and the hardness of the steel [18]. In this work the chemical composition effect on the structural, mechanical and tribological properties of the 316L composite was studied.

Cite this article as: Ben Zine, H. R., Balázsi, K., Balázsi, Cs. "The Effect of the Chemical Composition to the End-Properties of Ceramic Dispersed Strengthened 316L/Y_2O_3 Composites", Periodica Polytechnica Chemical Engineering, 2019. https://doi.org/10.3311/PPch.13591

2 Experimental methods

The austenitic 316L stainless steel powder from Höganäs with 16.8Cr–12Ni–2.5Mo–1.5Mn–0.6Si elemental composition and with average grain size ~70 μm and the Y_2O_3 powder grade C from H.C. Starck with ~700 nm in average particle size have been used to prepare two composites: 316L/0.33 wt% Y_2O_3 and 316L/1 wt% Y_2O_3. The Union Process attritor mill type 01-HD/HDDM has been used in order to reduce the steel grains size and insure a homogeneous distribution of the ceramic particles in the steel matrix. The composite powders have been elaborated by milling in ethanol for 5 hours at 600 rpm using 3 mm stainless steel balls with ball/material weight ratio of 10:1. The composites have been sintered under 50 MPa mechanical pressure at 900 °C for 5 minutes dwelling time in vacuum using the Sinter-SPS-7.40MK-VII apparatus in Istanbul Technical University. The sintered samples were solid disks with 100mm in diameter and ~9 mm thickness. The composites density has been measured using Archimedes method. The tribological properties of sintered samples have been investigated using the setup type CSM-HT-Tribometer. Different grinding papers (grade up to 100 μm) have been used for polishing the samples before measuring the tribological properties. 5 N normal load was applied with the 5 mm diameter Si_3N_4 ball against the steel sample surface with 1mm shift from the rotation axe of the sample. The samples have been tested for 2161 m at room temperature in air at 47 % atmosphere humidity for the 0.33 wt% Y_2O_3 and 53 % for the 1wt% Y_2O_3. The wear track was investigated by Keyence Microscope for wear volume calculations. The structure and morphology of the milled powders have been investigated using the scanning electron microscopy (SEM, Zeiss-SMT LEO 1540 XB and Jeol JSM-25-SIII) equipped with EDS. The X-ray diffractometer Bruker AXS D8 with CuKα radiation have been used to analyze the phases in the two composites. The Philips CM20 Transmission Electron Microscope (TEM) operated at 200 kV acceleration voltage has been used to investigate the composites microstructures, discs with 3 mm diameter and 20 μm thickness in the centre have been prepared by mechanical thinning, polishing, and dimpling. Technoorg Linda ionmill has been used to reach electron transparency thickness, 10 keV Ar+ ions at an incidence angle of 5° with respect to the surface. In the final period of the milling process, the ion energy was decreased gradually to 3 keV to minimize ion-induced structural changes in the surface layers. The TEM images were taken in plan view. The hardness of the sintered composites has been measured by Vickers method where 5 N was applied for 10 seconds.

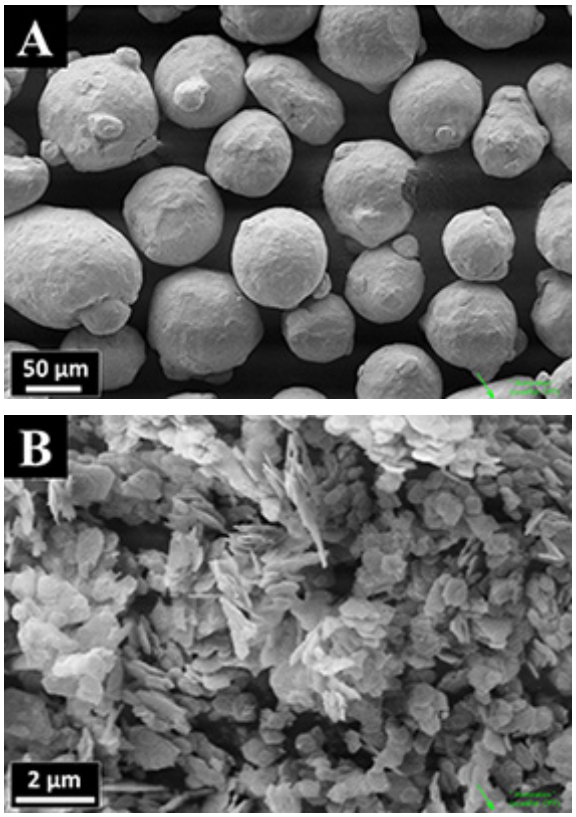

Fig. 1 SEM images of the starting powders. A) 316L, B) Y_2O_3.

3 Results

3.1 Morphological and Structural investigation

The investigation of the atomised 316L stainless steel starting powder by SEM (Fig. 1A) shows that it is consisted of ~70 μm globular shape grains with the presence of satellites on their surface. The Y_2O_3 powder (Fig. 1B) is consisting of flake-like shaped grains with ~700 nm particle size in average. The globular shape grains of 316L starting powder has been transformed into 4 types/shapes (as in Fig. 2, 1-slightly damaged, 2-flattened, 3-flake-like shape and 4-small broken grains) due to the high impact forces implemented by the steel balls during the 5 hours milling. The impact of steel balls is higher in the bottom part of the milling jar comparing the top part, that is why we have different grains morphologies.

The small grains (Fig. 2 spot 4) are broken flake-like shape steel grains, we assume that more 1-2 hours in addition of attrition milling would make a significant grain size reduction.

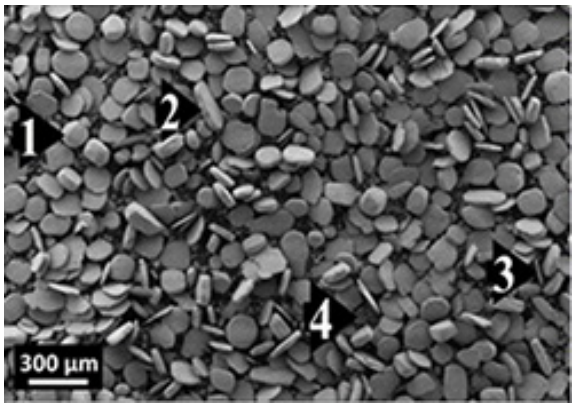

Fig. 2 SEM image of the starting milled 316L powder. 1- slightly damaged, 2- flattened, 3- flake-like shape, 4- small broken grains.

The ratio of flake-like shape grains to the flattened and slightly damaged grains is bigger in the case of the Y_2O_3 additions (Fig. 3A and Fig. 4A) comparing to milled 316L powder (Fig. 2).

The presence of the Y_2O_3 in the case of the 316L/0.33wt% Y_2O_3 was not clearly detectable, therefore, we investigated the surfaces of grains at high magnifications (Fig. 3B), the EDS spectras (Fig. 3C) shows the presence of yttria in all of the selected spots. The Aluminum presence is a contamination trace in the starting 316L powder (as received from Höganäs company). In the case of the 316L/1 wt% Y_2O_3, the EDS spectra clearly show the yttria presence in the milled composite powder (Fig. 4B). The yttria particles were embedded into the surface of the 316L steel grains making it harder, this increased the impact of milling balls which in turn increased the evolution of flake-like grains.

The milling efficiency was slightly decreased in the case of the 316L/1 wt% Y_2O_3 composite comparing to the 316L/0.33 wt% Y_2O_3 because the yttria particles agglomerated together which influenced (decreased) the milling efficiency.

The XRD results (Fig. 5) confirmed that the 316L starting powder is an austenitic powder of ɣ-Fe_3Ni_2 phase (JPC2:03-065-5131) with main lines of (2θ= 43.532°, 50.705°, 74.535°). After milling we noticed the presence of the ferrite α-Fe phase (JCP2: 03-065-4899) with the main lines of (2θ= 44.663°, 65.008°). The Y_2O_3 main lines (JCP2: 00-041-1105, 2θ= 29.150°, 48.541°) was clearly detected in the case of the 316L/1 wt% Y_2O_3 milled powder. The peak at 2θ= 69° is the Si peak of the used sample holder.

After the sintering process, the ferritic α-Fe phase has been transformed to the austenitic ɣ-Fe_3Ni_2 phase as it was expected. The Y_2O_3 peaks disappeared after sintering. In the case of the reference 316L sample we noticed

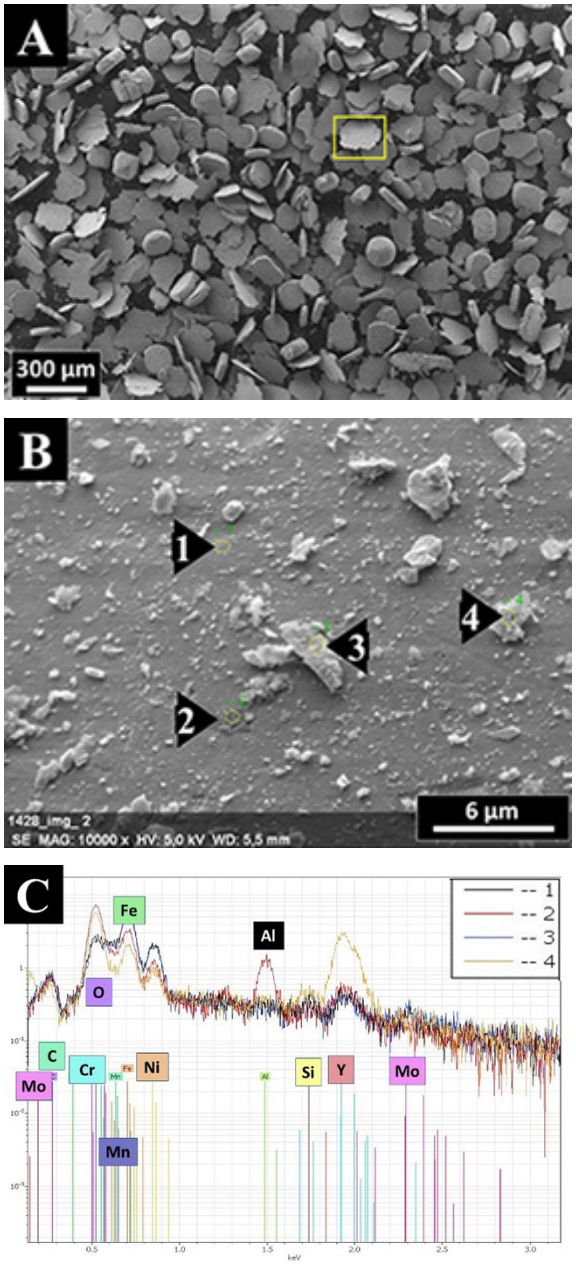

Fig. 3 Investigation of the milled 316L/0.33 wt% Y_2O_3 powder mixture. A) SEM image, B) Higher magnification of the selected zone in Fig 3A, C) EDS spectras of the selected zones in Fig3B.

a reorientation in the direction [200] of the grains after sintering.

The EDS spectra of the sintered 316L/0.33 wt% Y_2O_3 (Fig. 6) show the presence of small amount of Y_2O_3 in the composite. This finding is indicating some kind of diffusion or agglomeration of the yttria particles in the steel matrix, resulting in the decrease of the Y peak intensity in the sintered composite comparing the milled powders.

The Y peak was not detectable by EDS in the case of the sintered 316L/1 wt% Y_2O_3 (Fig. 7B). The Y peak is

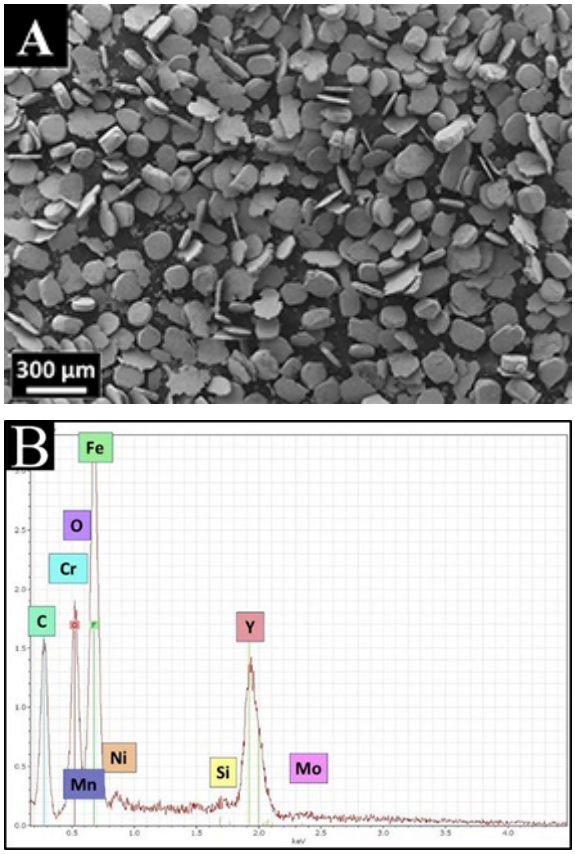

Fig. 4 Investigation of the milled 316L/1 wt% Y_2O_3 powder mixture. A) SEM image, B) EDS spectra.

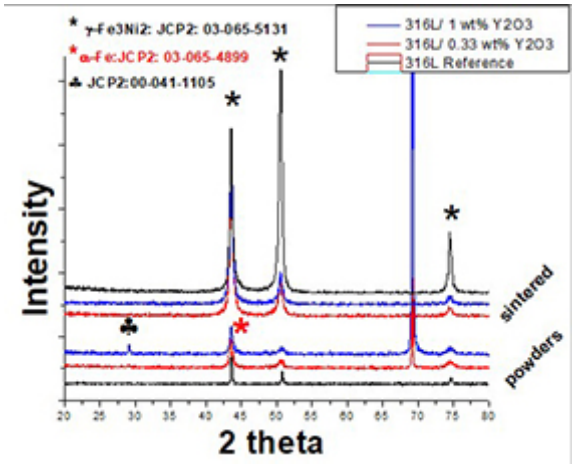

Fig. 5 XRD diffractorgarms of the starting 316L powder, milled powder mixtures and sintered composites.

not observed even with its higher content in this composite as a result of the non-homogeneous distribution of the yttria in the steel matrix. Presumably the Y peak can not be observed on EDS because the agglomeration of yttria particles during the sintering process (Fig. 7B).

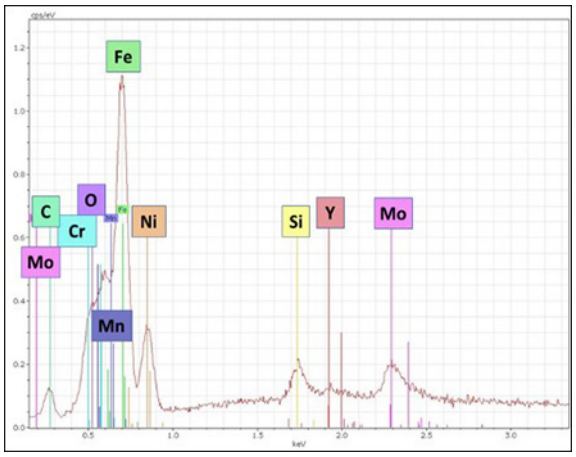

Fig. 6 EDS spectra of sintered 316L/0.33 wt% Y_2O_3.

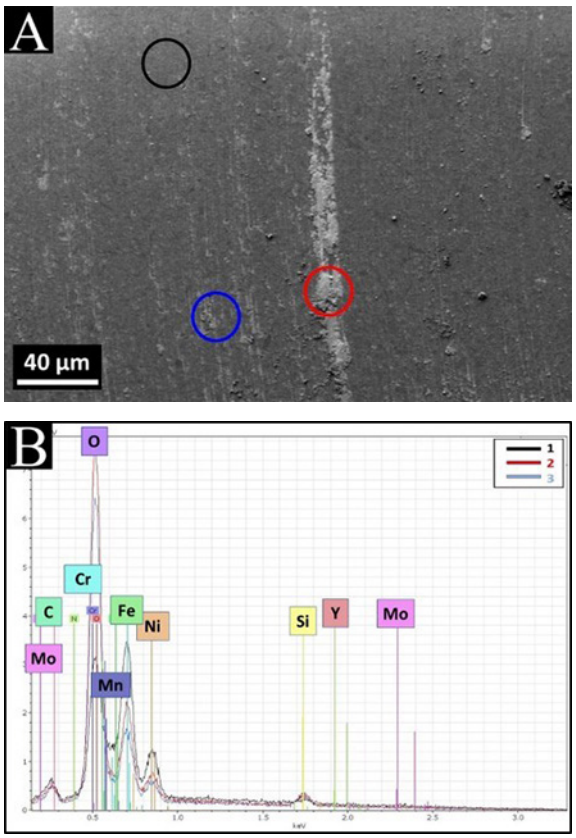

Fig. 7 Investigations of the sintered 316L/1 wt% Y_2O_3 composite. A) SEM image, B) EDS spectra.

The Fig. 8 and Fig. 9 show the TEM images of the sintered composites. In the case of the 316L/0.33 wt% Y_2O_3 (Fig. 8) we observed that the material is composed of relatively small steel grains of ~ 5-20µm with a good and homogeneous distribution of the Y_2O_3 in the grain boundaries, unlike the 316L/1 wt% Y_2O_3 (Fig. 9) where the yttria particles are agglomerated together. Micrometer

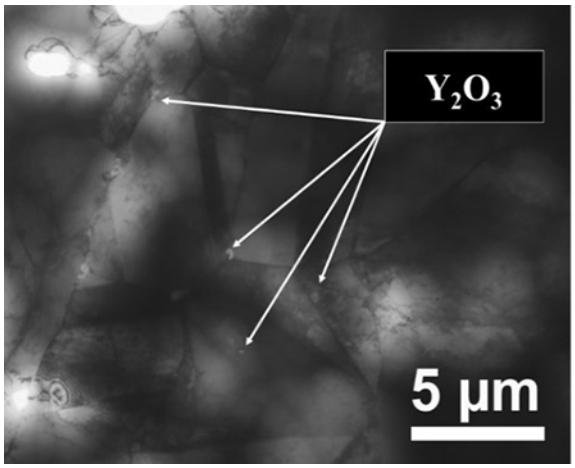

Fig. 8 TEM image of the sintered 316L/0.33 wt% Y_2O_3.

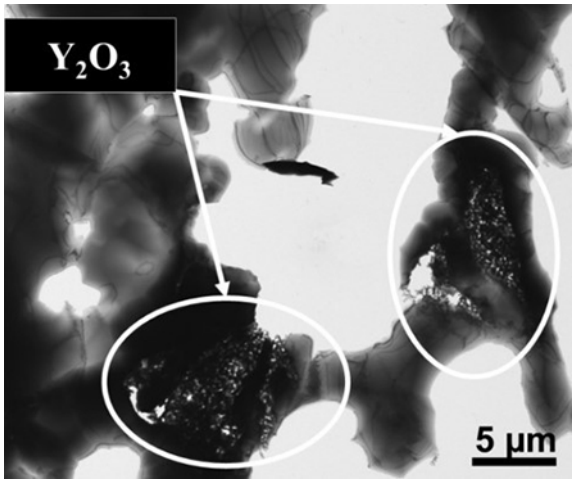

Fig. 9 TEM image of the sintered 316L/ 1 wt% Y_2O_3.

Table 1 Wear rate of the sintered composites.

Material	316L	316L/0.33 wt% Y_2O_3	316L/1 wt% Y_2O_3
Wear rate (m^2/N)	1.36177E-4	5.39844E-14	2.40614E-14

sized twinned regions can be distinguished in the steel grains in both composites.

After tribology investigation both Si_3N_4 ball and the samples surfaces have been damaged. The damage on the ball was insignificant. The wear track width and depth have been measured for wear volume calculation. The wear rate of the 316L reference, 316L/ 0.33 wt% Y_2O_3 and the 316L/ 1 wt% Y_2O_3 have been calculated (Table 1).

The wear rate has been reduced significantly with the addition of yttria to the matrix. The investigation of the damaged surfaces shows the formation of tribo films on the samples surfaces (Fig. 10A and Fig. 11A). No yttrium content was detected by EDS on the wear track of the two

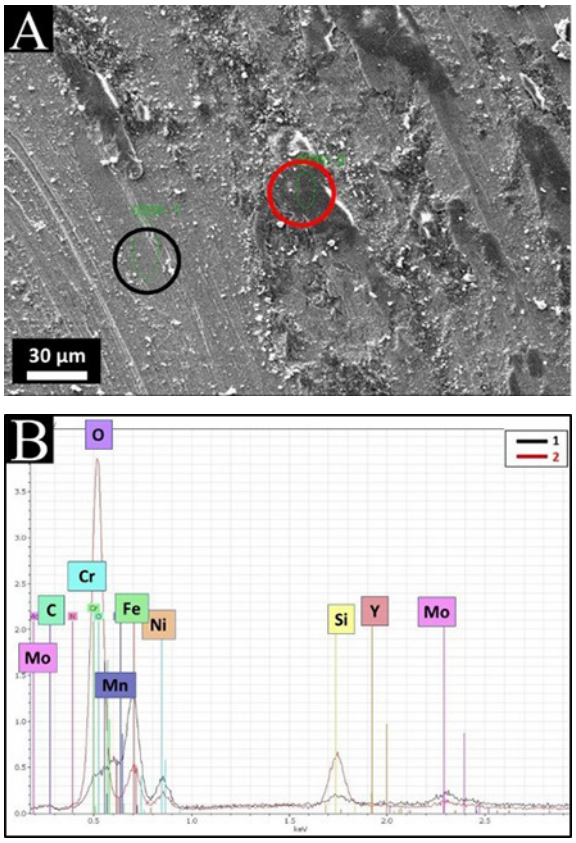

Fig. 10 Investigations of the sintered 316L/0.33 wt% Y_2O_3 composite. A) SEM image, B) EDS spectra.

composites (Fig. 10B and Fig. 11B). High intensity peaks of oxygen and silicon were measured in the same spot of the tribo-film in both composites, which can be explained by the formation of silicon oxide during the tribology test.

Silicon oxide formation is a result of temperature increase in the contact zone as a result of a relatively high sliding speed. The lower intensity peaks of the 316L components in zone 2 (Fig 10B and 11B) is due the coverage of 316L composite by the tribo-film. The friction coefficients are represented in Fig. 12.

The 316L/Y_2O_3 composites are showing higher density comparing with the 316L/Si_3N_4 composite elaborated using the same parameters [19]. The 316L/Y_2O_3 composites are harder than the 316L reference sample as it is represented in Fig 12. The HV values: 1.75±0.05, 2.63 ± 0.32 and 2.33 ± 0.165 GPa have been measured for the 316L (reference), 316L/0.33wt% Y_2O_3 and the 316L/1 wt% Y_2O_3 respectively. The 316L/ 0.33wt% Y_2O_3 composite was showing somewhat higher hardness values than the 316L/1 wt% Si_3N_4 composite from our previous work [20]. The friction coefficient dropped with addition

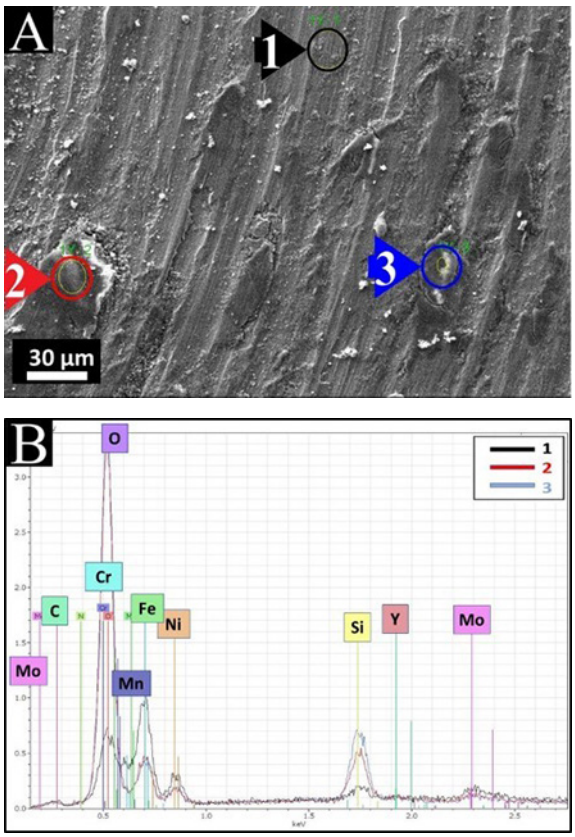

Fig. 11 Investigation of 316L/1 wt% Y_2O_3 sintered composite after tribological measurements. A) SEM image, B) EDS spectra.

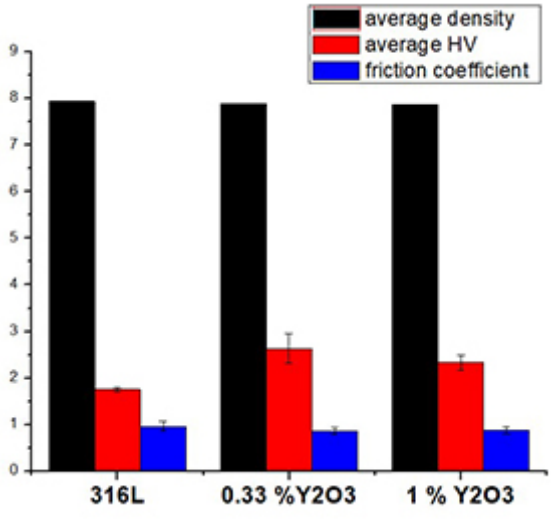

Fig. 12 Mechanical properties of composites vs. 316L reference.

of Y_2O_3. 0.962 ±0.108 was registered for the 316L reference sample, 0.863±0.078 for the 316L/ 0.33wt% Y_2O_3 and 0.806±0.083 for the 316L/1 wt% Y_2O_3.

4 Discussions

4.1 Morphological properties

The milling efficiency has been improved with the addition of the yttria as it observed clearly in Fig. 3A and Fig. 4A where the ratio of the flake-like shape grains to the slightly damaged and flattened grains is higher comparing the milled reference 316L powder (Fig. 2). This improvement in the milling efficiency is attributed to the yttria addition which increased impact effect by hardening surface of the steel grains. The EDS spectra of the milled powder with high intensity yttrium peak (Fig. 4B) and the milled powder X-ray diffractograms (Fig. 5) show the presence of Y_2O_3 in the 316L/1 wt% Y_2O_3 composite. In the case of sintered samples no yttria peaks in the XRD and EDS may be observed (Fig. 5 and Fig. 7B respectively). This finding proves that the agglomeration of the yttria particles in the 316L/1 wt% Y_2O_3 composite (Fig. 9) took place during the sintering process.

4.2 Structural properties

The presence of the ferrite α-Fe phase in the milled composites might be a result of an austenitic-martensitic/ferritic transformation during the milling process due to the sever deformation under the high impact of the milling balls or might be related to contamination from the milling setup. The ferrite phase was transformed to the ɣ-Fe_3Ni_2 as it is shown in Fig. 5. Two main lines of yttria has been clearly identified in the case of the 316L/1 wt% Y_2O_3 (Fig. 5) unlike in the case of the 316L/ 0.33 wt% Y_2O_3 where the yttria content was under the detection limit. The distribution of the yttria particles in the 316L/1 wt% Y_2O_3 composite is not homogeneous as we can observe in Fig. 9. The agglomeration of yttria shown in TEM results is in correlation with the XRD results (Fig. 5) and it explains the disappearance of the yttria peak in diffractogram of the 316L/1 wt% Y_2O_3 sintered composite.

4.3 Mechanical properties

The presence of yttria slightly dropped the density, however, the 316L/Y_2O_3 composites are showing higher densities comparing to similar composites made by the 3-Dimensional Fiber Deposition (3DFD) technique even when higher sintering temperatures were applied [12]. The prepared 316L/Y_2O_3 composites are showing higher hardness values comparing to the 316L/0.4 wt% Y_2O_3 prepared by electron beam selective melting (EBSM) and Spark Plasma Sintering even

after hot rolling [21]. The lower HV value of the 316L/1 wt% Y_2O_3 comparing to the 316L/0.33 wt% Y_2O_3 (Fig. 12) is due to the non-homogeneous distribution of the yttria particles (Fig. 9). The lower friction coefficient in the case of the 316L/Y_2O_3 composites comparing to the 316L reference sample is due to their higher hardness.

5 Conclusions

The elaboration of yttria dispersed strengthened steel using attrition milling and Spark Plasma Sintering has been demonstrated. The effect of changing chemical composition by addition of yttria to the 316L matrix on the structural and mechanical properties has been studied. The addition of yttria improved the milling efficiency. Agglomeration of the yttria particles took place during the sintering process in the case of the 316L/1wt% Y_2O_3. The 316L hardness and tribological properties have been improved with the addition of yttria. The 316L/0.33wt% Y_2O_3 show better mechanical properties comparing to the 316L/1wt% Y_2O_3 and the 316L reference samples.

Acknowledgement

Mr. Haroune Rachid Ben Zine thanks to Hungaricum Stipendium and MTA EK project "Nanostructural ODS steel development" for support. The authors acknowledge the excellent contribution to Dr. Zsolt E. Horváth (XRD), Dr. Zsolt Czigány (TEM), Prof. Filiz Cinar Sahin (SPS), Mr. Levente Illés (SEM/EDS) and Dr. Ákos Horváth to the experimental and evaluation. Thanks are due to Hungarian-Japanese Bilateral project "Development of electromagnetic non-destructive evaluation method for aging degradation of chromium steels at high temperatures".

References

[1] Zou, J., Grasso, S., Liu, L-F., Ma, H-B., Reece, M., Binner, M. "Flash spark plasma sintering of HfB_2 ceramics without pre-sintering", Scripta Materialia 156, pp. 115–119, 2018. https://doi.org/10.1016/j.scriptamat.2018.07.026

[2] Mahaseni, Z. H., Germi, M. D., Ahmadi, Z., Asi, M. S. "Microstructural investigation of spark plasma sintered TiB_2 ceramics with Si_3N_4 addition", Ceramics International, 44(11), pp. 13367–13372, 2018. https://doi.org/10.1016/j.ceramint.2018.04.171

[3] Velmurugan, C., Senthilkumara, V., Biswas, K., Yadavbet, S. "Densification and microstructural evolution of spark plasma sintered NiTi shape memory alloy", Advanced Powder Technology, 29(10), pp. 2456–2462, 2018. https://doi.org/10.1016/j.apt.2018.06.026

[4] Lang, E., Madden, N., Smith, C., Krogstad, J., Allaain, J. P. "Microstructural and compositional effects of transition metal carbide additions on dispersion-strengthened tungsten fabricated via spark plasma sintering", International Journal of Refractory Metals and Hard Materials, 75, pp. 279–286, 2018. https://doi.org/10.1016/j.ijrmhm.2018.04.015

[5] Wei, K., Nolas, G. S. "Enhanced thermoelectric properties of polymer/inorganic bulk composites through EG treatment and spark plasma sintering processing", Scripta Materialia, 150, pp. 70–73, 2018. https://doi.org/10.1016/j.scriptamat.2018.03.001

[6] Lucas, R., Davis, C. E., Clegg, W. J., Pizon, D., Babonneau, F., Foucaud, S., Antou, G., Maître, A. "Elaboration of ZrC-SiC composites by spark plasma sintering using polymer-derived ceramics", Ceramics International, 40(10), Part A, pp. 15703–15709, 2014. https://doi.org/10.1016/j.ceramint.2014.07.093

[7] Balázsi, C., Gillemot, F., Horváth, M., Wéber, F., Balázsi, K., Cinar Sahin, F., Onüralp, Y., Horváth, A. "Preparation and structural investigation of nanostructured oxide dispersed strengthened steels", Journal of Materials Science, 46(13), pp. 4598–4605, 2011. https://doi.org/10.1007/s10853-011-5359-1

[8] Kishore Kumar, P., Sai, N. V., Krishna, A. G. "Effect of Y_2O_3 addition and cooling rate on mechanical properties of Fe-24Cr-20Ni-2Mn steels by powder metallurgy route", Composites Communications, 10, pp. 116–121, 2018. https://doi.org/10.1016/j.coco.2018.09.003

[9] Yang, J., Trapp, J., Guo, Q., Kieback, B. "Joining of 316L stainless steel by using spark plasma sintering method", Materials & Design (1980-2015), 52, pp. 179–189, 2013. https://doi.org/10.1016/j.matdes.2013.04.091

[10] Raja, A., Upadhyaya, A., Agrawal, D. K. "Effect of heating mode and Y2O3 addition on electrochemical response on austenitic and ferritic stainless steels, Corrosion Engineering", Science and Technology, 50(2), pp. 91–102, 2015. https://doi.org/10.1179/1743278214Y.0000000176

[11] Peruzzo, M., Beux, T. D., Ordoñez, M. F. C., Souza, R. M., Farias, C. M. "High-temperature oxidation of sintered austenitic stainless steel containing boron or yttria", Corrosion Science, 129, pp. 26–37, 2017. https://doi.org/10.1016/j.corsci.2017.09.002

[12] Verhiestade, K., Mullens, S., De Wispelaere, N., Claessens, S., DeBremaecker, A., Verbeken, K. "Nano-yttria dispersed stainless steel composites composed by the 3 dimensional fiber deposition technique", Journal of Nuclear Materials, 428(1–3), pp. 54–64, 2012. https://doi.org/10.1016/j.jnucmat.2012.01.025

[13] Verhiest, K., Almazouzi, A., DeWispelaere, N., Petrov, R., Claessens, R. "Development of oxides dispersion strengthened steels for high temperature nuclear reactor applications", Journal of Nuclear Materials, 385(2), pp. 308–311, 2009. https://doi.org/10.1016/j.jnucmat.2008.12.006

[14] Lindau, R., Möslang, A., Schirra, M., Schlossmacher, P., Klimenkov, M. "Mechanical and microstructural properties of a hipped RAFM ODS-steel", Journal of Nuclear Materials, 307-311, pp. 769–772, 2002.

https://doi.org/10.1016/S0022-3115(02)01045-0

[15] Baek, S-W., Song, E. J., Hyun Kim, J., Lee, Y-H., Ryu, K. S., Kim, S-W. "Hydrogen susceptibility of nano-sized oxide dispersed austenitic steel for fusion reactor", Fusion Engineering and Design, 121, pp. 105–110, 2017. https://doi.org/10.1016/j.fusengdes.2017.06.027

[16] Hutař, P., Kuběna, I., Ševčík, M., Šmíd, M., Kruml, T., Náhlíka, L. "Small fatigue crack propagation in Y2O3 strengthened steels", Journal of Nuclear Materials, 452(1–3), pp. 370–377, 2014. https://doi.org/10.1016/j.jnucmat.2014.05.07

[17] Kumar, P. K., Sai, N. V., Krishna, A. G. "Effect of Y2O3 and ZrO2 on the microstructure and mechanical properties of nano-ODS 21Cr-9Mn-6Ni steels", Materials and technology, 52(4), pp. 493–497, 2018. https://doi.org/10.17222/mit.2017.199

[18] Sun, D., Liang, C., Shang, J., Yin, J., Song, Y., Li, W., Liang, T., Zhang, X. "Effect of Y2O3 contents on oxidation resistance at 1150 °C and mechanical properties at room temperature of ODS Ni-20Cr-5Al alloy", Applied Surface Science, 385, pp 587–596, 2016. https://doi.org/10.1016/j.apsusc.2016.05.143

[19] Ben Zine, H. R., Balazsi, K., Balazsi, C. "Effect of the α-Si_3N_4 addition on the tribological properties of 316L stainless steel prepared by attrition milling and spark plasma sintering", Anyagok Világa (Materials Word), 1, pp. 9–16, 2018. [online] Available at: http://anyagokvilaga.hu/2018_BenZine.pdf [Accessed: date (day month year)]

[20] Ben Zine, H.R., Cinar Sahin, F., Horváth, Z.E., Czigány, Zs., Horváth, Á., Balázsi, K., Balázsi, C. "Effect of Si_3N_4 addition on the morphological and structural properties of the 316L stainless steel for nuclear applications", Resolution and Discovery, 2(1), pp. 23–30, 2017. https://doi.org/10.1556/2051.2017.00055

[21] Gao, R., Ge, W., Miao, S., Zhang, T., Wang, X., Fang, Q. "Hot rolling and annealing effects on the microstructure and mechanical properties of ODS austenitic steel fabricated by electron beam selective melting", Frontiers of Materials Science, 10(1), pp. 73–79, 2016. https://doi.org/10.1007/s11706-016-0327-y